LETTER TO THE EDITOR

Structures of human bile acid exporter ABCB11 reveal a transport mechanism facilitated by two tandem substrate-binding pockets

Cell Research (2022) 0:1–4; https://doi.org/10.1038/s41422-021-00611-9

Dear Editor,

Bile acids are a group of cholesterol-derived physiological surfactants required for digestion of lipids and fat-soluble vitamins.[1] However, excess of bile acids is detrimental to metabolic homeostasis and bile acid imbalance can contribute to cancer progression.[2] Bile acids are produced primarily in the liver and then secreted to the bile duct before delivery to the small intestine,[3] where up to 95% of bile acids are reabsorbed and recirculated to the liver (Supplementary information, Fig. S1a). The primary bile acids are biosynthesized in hepatocytes via oxidation of cholesterol and modified by either taurine or glycine,[4] forming the conjugated primary bile acids which harbor a cholic acid moiety and a taurine/glycine moiety (Supplementary information, Fig. S1b). This enterohepatic circulation of bile acids is driven by a series of transmembrane transporters (Supplementary information, Fig. S1a), including the ATP-binding cassette (ABC) transporter ABCB11 (also termed bile salt export pump BSEP).[5]

ABCB11 is localized to the canalicular membrane and is the primary transporter responsible for the continuous excretion of bile acids from hepatocytes to the bile duct.[5] In clinic, mutations in the *ABCB11* gene have been associated with inherited diseases such as progressive familial intrahepatic cholestasis type 2 (PFIC2) and benign recurrent intrahepatic cholestasis type 2 (BRIC2).[6] Following our recently reported apo-form structure of human ABCB11,[7] we obtained the full-length human ABCB11 with various concentrations of taurocholate (TC) added before specimen preparation. Ultimately, we solved two cryo-EM structures of the substrate-bound ABCB11 both at 3.7 Å resolution, with one or two extra densities in the transport cavity in the presence of 100 μM or 1 mM TC (thus termed ABCB11-1 and ABCB11-2), respectively (Fig. 1a, b; Supplementary information, Figs. S2–S5, Table S1). Both complex structures adopt an inward-open conformation with two separated nucleotide-binding domains (NBD1 and NBD2) in the intracellular side, and two intertwined TMDs (TMD1 and TMD2), each of which consists of 6 transmembrane helices (TMs) and extends from membrane to interact with the corresponding NBD via two coupling helices, a typical feature of type-IV transporter.[8]

In the transport cavity of ABCB11-2, there are two extra densities: one located in the outer membrane leaflet (OML) and the other in the inner membrane leaflet (IML), which could be well fitted with two TC molecules (termed TC1 and TC2), respectively (Fig. 1a; Supplementary information, Fig. S3). The two TC molecules are not symmetrically bound to the pseudo-symmetric TMD1 and TMD2; rather, they are stacked against each other in a pose parallel to the membrane plane (Fig. 1a). In contrast, there is only one extra density in OML in the structure of ABCB11-1, which could be fitted with a TC molecule (Fig. 1b).

Received: 30 August 2021 Accepted: 20 December 2021
Published online: 18 January 2022

Structural superposition revealed that the two complex structures display a similar overall structure, with a root mean square deviation (RMSD) of 2.101 Å (Fig. 1c). TC1 in ABCB11-2 could be generally superimposed against the only one TC in ABCB11-1, except for a slight conformational change at the taurine moiety (Fig. 1d). Upon binding to TC2, the two NBDs of ABCB11-2 shift towards each other, with a distance of 4 Å smaller than that of ABCB11-1 (Fig. 1c); meanwhile, TM10 in ABCB11-2, which is a continuous helix in ABCB11-1, is unfolded into two short helices connected with a long loop from residues Thr917 to Ala932 (Fig. 1e). In consequence, an induced 180° rotation of the side chain of Arg920 enables it to form a salt bridge with the negatively-charged taurine moiety of TC2.

In the ABCB11-2 structure, two TC molecules are respectively bound to the pockets formed within the OML and IML. TC1 positioned within the OML pocket is deeply buried in the membrane, whereas TC2 in the IML pocket is somewhat exposed to the intracellular space. The two pockets are generally independent, despite connected in the middle and sharing a joint residue Trp330 that fixes the cholic acid moieties of both TC1 and TC2 (Fig. 1f).

For both TC1 and TC2, all the three hydroxyl groups of the steroid rings point towards TMD2, leaving the hydrophobic side of the steroid nucleus facing TMD1 (Fig. 1g, h; Supplementary information, Fig. S6a–e). In the OML pocket, residues Leu364, Ile367, Ile333, Phe334, Tyr337, and Trp330 undergo extensive hydrophobic interactions with the steroid nucleus of TC1 (Fig. 1g). The alkane chain of TC1 is embraced by a series of hydrophobic residues (Ile367, Leu364, Phe83, and Val79), whereas its taurine moiety is stabilized by Tyr145 via a hydrogen bond. Residues Phe83, Thr769, Met992, Asn996, Leu1026, and Ala1030 further outline the boundary of the OML pocket (Fig. 1g). In the IML pocket, the hydrophobic residues Ile259, Val329, Trp330 and Leu371 accommodate the steroid nucleus of TC2 on one side, while Arg1033 fixes the hydroxyl group at the 3rd position on the other side (Fig. 1h). The taurine moiety of TC2 is stabilized by salt bridges with two positively-charged residues (Arg920 and Arg223), in addition to a hydrogen bond with Arg223. Notably, the indole ring of Trp330, the aforementioned joint residue contributes to the hydrophobic interactions with the steroid nucleus of both TC1 and TC2 (Fig. 1g, h).

Multiple-sequence alignment revealed that most residues comprising the two TC-binding pockets are conserved among ABCB11 homologs (Supplementary information, Fig. S6f), suggesting a universal feature of a two-pocket transport cavity. The electrostatic surface properties of the TC-binding pockets showed a generally hydrophobic environment surrounding the entire TC1 molecule, in contrast to a positively-charged potential towards the

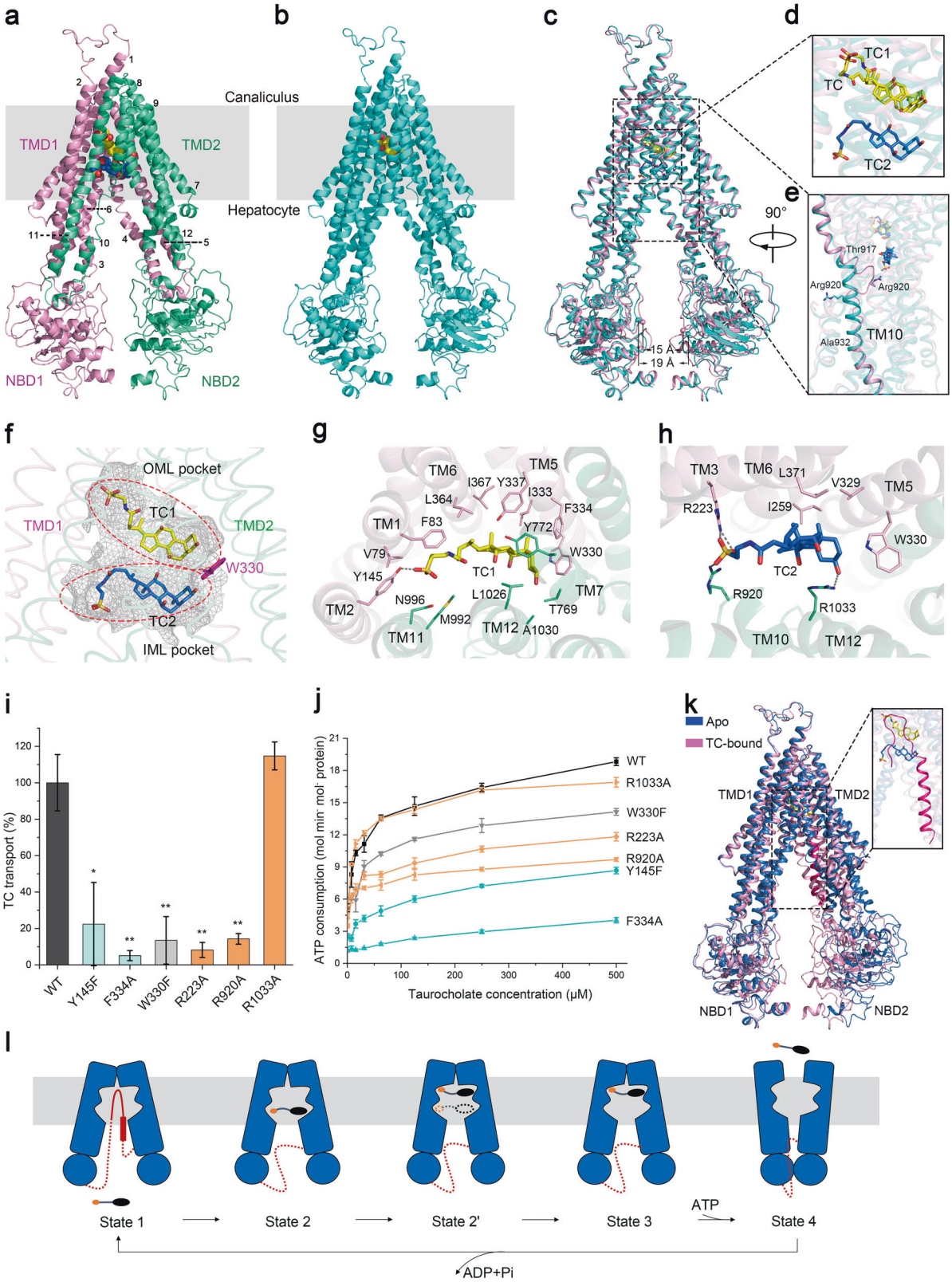

taurine moiety of TC2 (Supplementary information, Fig. S7). It appears that the positively-charged residues Arg223 and Arg920 in the IML pocket contribute to the recognition of TC's hydrophilic taurine moiety (Fig. 1h), while the hydrophobic residues in the OML pocket provide a highly complementary space for interaction with TC's hydrophobic cholic acid moiety (Fig. 1g).

We further respectively mutated the conserved residues constituting the pockets and performed the transport activity

Fig. 1 Structure determination and biochemical analysis of substrate-bound ABCB11. a, **b** The overall structures of ABCB11 in complex with two TCs (ABCB11-2) (**a**) and one TC (ABCB11-1) (**b**), respectively. The numbering in **a** refers to the TM helices. TC molecules are colored in yellow and blue, respectively. **c** Superposition of ABCB11-1 against ABCB11-2. Distances between the Walker A motif and the signature motif are indicated. **d**, **e** Details of conformational changes at TC-binding pockets (**d**) and TM10 (**e**). **f** Contour of two TC molecules bound in the pockets illustrated by PyMOL. The outlines of OML and IML pockets are shown in circles of dashed lines. **g**, **h** TC-binding patterns in the OML pocket (**g**) and the IML pocket (**h**). Hydrogen bonds and salt bridges are shown as black dashed lines. **i**, **j** Transport activity assays (**i**) and ATPase activity assays (**j**) of ABCB11 wild type and mutants in the OML and the IML pockets. The activity of wild-type ABCB11 (black) was set as 100%. Data are presented as means ± SD. One-way analysis of variance is used for the comparison of statistical significance. $^{*}P < 0.05$; $^{**}P < 0.01$; $^{***}P < 0.001$. **k** Superposition of ABCB11-2 (pink) against the apo-form ABCB11 (indigo). The inter-domain linker of apo-form ABCB11 is colored in red. **l** The five states of ABCB11 in the transport cycle are sequentially labeled. The inter-domain linker is shown in red. The taurine moiety of TC is shown as an orange sphere, and the cholic acid moiety is shown as a black ellipse.

assays. All mutants displayed similar profiles in gel filtration with the wild type, indicating they are well-folded (Supplementary information, Fig. S6g). Mutations of residues at the OML pocket (Y145F and F334A) and IML pocket (R223A and R920A), or substitution of the joint residue Trp330 with Phe, led to a drastic decrease of transport activity (Fig. 1i). Unexpectedly, the ABCB11^{R1033A} variant did not display significant change in transport activity, despite a hydrogen bond between Arg1033 and TC2, suggesting that hydrophobic interactions, rather than this hydrogen bond, with the cholic acid moiety are determinant to TC2 binding.

We compared the ATPase activities of the mutants and the wild type upon stimulation with different concentrations of TC. In general, all mutations in the pockets led to a somewhat decreased ATPase activity at a given TC concentration, except for R1033A that maintains a transport activity similar to the wild type (Fig. 1j). Notably, mutations of residues (Y145F and F334A) in the OML pocket, in addition to R920A, resulted in a much sharper decrease of ATP consumption rate, whereas the two mutations (R223A and R1033A) in the IML pocket, as well as the joint residue mutation W330F, had slight effect on the ATPase activity (Fig. 1j).

In our previously reported apo-form structure of ABCB11, we found an extra density in the transport cavity which was tentatively fitted with the N-terminus.[7] Thanks to the recently released non-uniform refinement program from cryoSPARC,[9] we reprocessed our cryo-EM data of apo-form ABCB11, and obtained a density map of higher resolution in the transport cavity. It is more convincing to fit the NBD1–TMD2 linker (residues from Ser686 to Ser719) in this density (Supplementary information, Fig. S8a). In fact, a 3.6 Å structure of the N-terminus-truncated ABCB11 also possesses a similar density in the transport cavity (Supplementary information, Fig. S9), further excluding the possibility that the N-terminus accounts for the extra density. Remarkably, the inter-domain linker is missing in both complex structures (Fig. 1a, b), most likely being repelled upon substrate binding (Fig. 1k). Structural comparison of ABCB11-2 with the apo form revealed obvious induced fit upon substrate binding, with an overall RMSD of 5.173 Å (Fig. 1k; Supplementary information, Fig. S10). Compared to the wild type, the linker-truncated version which is well-folded according to its gel filtration profile, namely ABCB11$^{\Delta 686–720}$ possesses a residual transport activity of ~10% (Supplementary information, Fig. S8b, c), indicating that this linker is crucial for the transport activity. Moreover, the linker regions are highly conserved in both sequence and length, among ABCB11 homologs (Supplementary information, Fig. S11). Notably, there are several conserved positively charged arginine residues in the helix of the inter-domain linker. A mutant in two conserved arginine residues (R692A/R696A) showed significantly decreased ATPase activity compared to the wild type (Supplementary information, Fig. S8c). Thus, we speculate that the inter-domain linker may recruit the negatively charged substrates through the positively charged arginine residues.

In sum, ABCB11 possesses two tandem substrate-binding pockets with an affinity gradient in its TMD, which can serve as a unidirectional cavity. Most of the residues that compose the two pockets are conserved in ABCB11 homologs from all vertebrates that possess the bile acid transport pathway (Supplementary information, Fig. S6f). Different from ABCB1 which shares 50% sequence identity with ABCB11 and binds to a broad spectrum of substrates,[10] ABCB11 predominately transports conjugated primary bile acids. It seems plausible that this two-pocket structure enables ABCB11 to more precisely distinguish the two moieties of conjugated primary bile acids when compared with the single substrate-binding pocket of the apical sodium-dependent bile salt transporter (ASBT), which is known to recognize the cholic acid moiety of conjugated/unconjugated primary or secondary bile acids (Supplementary information, Fig. S1a).[11] The IML pocket of ABCB11 provides two positively charged residues to recognize the taurine moiety of conjugated bile acids, whereas the OML pocket defines a space complementary in shape and charge with the cholic acid moiety. Both the OML and IML pockets of ABCB11 are occupied in the presence of 1 mM TC, a concentration far beyond the physiological concentration of ~60 μM in human liver,[12] whereas only the OML pocket is occupied upon the addition of 100 μM TC. Therefore, in the presence of overloaded TC, we captured a combination of two transient transport states. Our two complexed structures viewed in combination with structural analysis suggested a pocket-to-pocket transfer cascade that is driven by increasing substrate affinity from IML to OML. This pocket-to-pocket transfer mechanism is different from that of other known ABC transporters which possess two substrate-binding pockets. For instance, the ABCB7 homolog NaAtm1 from *Novosphingobium aromaticivoran* has two substrate-binding sites in the inner membrane leaflet, with the primary binding site towards the cytoplasmic side, and the second, of lower occupancy, positioned deeper in the membrane.[13] The recently reported structure of the cholesterol transporter ABCG5/G8 also revealed a second cholesterol-binding site, in addition to the binding site in the inner membrane leaflet.[14] This second binding site was obtained with oversaturated substrates. In both cases, the second site most likely displays lower substrate-binding affinity. Therefore, these two pockets of ABCB11 define a unidirectional substrate diffusion cavity employing a transfer mechanism that strongly resembles the long-known "facilitated diffusion" process, in which molecules adopt the passive movement along the concentration gradient in a selective manner.[15]

Thus, we propose that the two-pocket structure of ABCB11 provides a mechanism of facilitated diffusion in addition to ATP hydrolysis (Fig. 1l). At State 1, the inter-domain linker occupies the substrate-binding pockets. Upon substrate binding, the inter-domain linker is expelled. Afterwards, the positively-charged residues of the IML pocket recruit the taurine moiety of the intracellular substrate (State 2). The presence of overloaded TC enabled us to capture a transient state with two TC molecules simultaneously bound to the two pockets (State 2′). However, owing to higher affinity, the substrate preferentially diffuses from the IML to OML pocket (State 3). Eventually, the substrate is pumped out to the extracellular space upon ATP binding (State 4). After release of the substrate, hydrolysis of ATP resets ABCB11 to its rest state, ready for another cycle of transport.

Liang Wang[1,2,3], Wen-Tao Hou[1,2,3]✉, Jie Wang[1,2], Da Xu[1,2], Cong Guo[1,2], Linfeng Sun[1,2], Ke Ruan[1,2], Cong-Zhao Zhou[1,2]✉ and Yuxing Chen[1,2]✉

[1]The First Affiliated Hospital of USTC, Division of Life Sciences and Medicine, University of Science and Technology of China, Hefei, Anhui, China. [2]School of Life Sciences, Division of Life Sciences and Medicine, University of Science and Technology of China, Hefei, Anhui, China. [3]These authors contributed equally: Liang Wang, Wen-Tao Hou. ✉email: todvince@mail.ustc.edu.cn; zcz@ustc.edu.cn; cyxing@ustc.edu.cn

DATA AVAILABILITY

All relevant data are available from the authors and/or included in the manuscript or Supplementary information. Atomic coordinates and EM density maps of the human ABCB11 with two TCs (3.7 Å, PDB: 7DV5; EMDB: 30870) and ABCB11 with one TC (3.7 Å, PDB: 7E1A; EMDB: 30938) in this paper have been deposited in the Protein Data Bank and the Electron Microscopy Data Bank, respectively. The EM density map of $ABCB11^{\Delta N44}$ has been deposited in the Electron Microscopy Data Bank (EMDB: 32261).

REFERENCES

1. Staels, B. & Fonseca, V. A. *Diabetes Care* **32**, S237–S245 (2009).
2. Li, T. & Apte, U. *Adv. Pharmacol.* **74**, 263–302 (2015).
3. Boyer, J. L. *Compr. Physiol.* **3**, 1035–1078 (2013).
4. Russell, D. W. *Annu. Rev. Biochem.* **72**, 137–174 (2003).
5. Trauner, M. & Boyer, J. L. *Physiol. Rev.* **83**, 633–671 (2003).
6. Davit-Spraul, A., Gonzales, E., Baussan, C. & Jacquemin, E. *Orphanet J. Rare Dis.* **4**, 1 (2009).
7. Wang, L. et al. *Cell Res.* **30**, 623–625 (2020).
8. Thomas, C. & Tampe, R. *Annu. Rev. Biochem.* **89**, 605–636 (2020).
9. Punjani, A., Zhang, H. & Fleet, D. J. *Nat. Methods* **17**, 1214–1221 (2020).
10. Alam, A., Kowal, J., Broude, E., Roninson, I. & Locher, K. P. *Science* **363**, 753–756 (2019).
11. Hu, N. J., Iwata, S., Cameron, A. D. & Drew, D. *Nature* **478**, 408–411 (2011).
12. Setchell, K. D. et al. *Gastroenterology* **112**, 226–235 (1997).
13. Lee, J. Y., Yang, J. G., Zhitnitsky, D., Lewinson, O. & Rees, D. C. *Science* **343**, 1133–1136 (2014).
14. Sun, Y. et al. *Proc. Natl. Acad. Sci. U.S.A.* **118**, e2110483118 (2021).
15. Carruthers, A. *Physiol. Rev.* **70**, 1135–1176 (1990).

ACKNOWLEDGEMENTS

We thank Dr. Yongxiang Gao at the Center for Integrative Imaging, Hefei National Laboratory for Physical Sciences at the Microscale, University of Science and Technology of China during cryo-EM image acquisition. We thank Mr. Jishu Ren at the Isotope Laboratory, University of Science and Technology of China for the transport assays. We also thank Prof. Huaqiang Xu at Shanghai Institute of Materia Medica, Chinese Academy of Sciences for the assistance with paper revision. This work was supported by the Ministry of Science and Technology of China (2019YFA0508500), the Strategic Priority Research Program of the Chinese Academy of Sciences (XDB37020202), and the Fundamental Research Funds for the Central Universities (YD20700002005).

AUTHOR CONTRIBUTIONS

Y.C. and C.Z.Z. conceived the project and designed the experiments. L.W., J.W., and C.G. expressed and purified human ABCB11. L.W. performed initial negative-staining and cryo-EM analyses and prepared all grids. L.W., W.T.H. and K.R. performed functional assays. L.W. and D.X. performed cryo-EM data collection. L.W. and L.S. performed ABCB11 structure determination and model refinement. W.-T.H., L.W., C.Z.Z. and Y.C. wrote the manuscript.

COMPETING INTERESTS

The authors declare no competing interests.

ADDITIONAL INFORMATION

Supplementary information The online version contains supplementary material available at https://doi.org/10.1038/s41422-021-00611-9.

Correspondence and requests for materials should be addressed to Wen-Tao Hou, Cong-Zhao Zhou or Yuxing Chen.

Reprints and permission information is available at http://www.nature.com/reprints